J. Mod. Power Syst. Clean Energy (2013) 1(3):249–257
DOI 10.1007/s40565-013-0034-y

Stability of interacting grid-connected power converters

Cheng WAN, Meng HUANG, Chi K. TSE (✉), Xinbo RUAN

Abstract The power grid in a typical micro distribution system is non-ideal, presenting itself as a voltage source with significant impedance. Thus, grid-connected converters interact with each other via the non-ideal grid. In this study, we consider the practical scenario of voltage-source converters connected to a three-phase voltage source with significant impedance. We show that stability can be compromised in the interacting converters. Specifically, the stable operating regions in selected parameter space may be reduced when grid-connected converters interact under certain conditions. In this paper, we develop bifurcation boundaries in the parameter space with respect to Hopf-type instability. A small-signal model in the *dq*-frame is adopted to analyze the system using an impedance-based approach. Moreover, results are presented in design-oriented forms so as to facilitate the identification of variation trends of the parameter ranges that guarantee stable operation.

Keywords Power converters, Stability analysis, Interacting systems, Grid-connected converters

1 Introduction

Three-phase pulse-width-modulated (PWM) voltage-source converters (VSCs) operating in rectifier mode have become a popular choice for ac-dc power conversion in many medium to high power applications. Due to the many desirable features that the VSC offers, e.g., low current harmonics, controllable power quality, and high efficiency, the VSC has been used in a variety of industrial and commercial applications, such as un-interruptible power supply systems, power supplies for telecommunication equipment, HVDC systems, distributed energy sources for renewable energy generation, battery storage systems, power conversion systems for process technology, and so on [1]. In most of these applications, the VSC does not only function as a high-performance power load to the ac power source, but also a reliable interface for many power conversion systems with the ac source.

As possibilities of applications of VSCs increase, it can be appreciated that multiple VSCs may connect to the power grid at a so-called point of common coupling (PCC), while each VSC works under its own specific condition and application, as shown in the usual representation of Fig. 1 [2]. The same structure is also employed in some specific application scenarios, including aircraft power systems [3], shipboard power systems [4], micro grids [5], etc. As each converter is designed separately for its own load condition, the mutual coupling in practice via the grid may pose a stability concern as the grid is non-ideal in reality and presents at the point of common coupling a significant amount of impedance which is not always predictable. As a result, the stability of the system should be considered with the coupled system model in mind rather than the unrealistic though simple model where each converter is assumed to behave independently.

For the purpose of illustrating the effect of mutual coupling, it suffices to consider two converters under the structure shown in Fig. 2. To maintain generality of our

Received: 9 September 2013 / Accepted: 30 October 2013 / Published online: 7 December 2013

C. WAN, State Key Laboratory of Advanced Electromagnetic Engineering and Technology, Huazhong University of Science and Technology, Wuhan, China
C. WAN, M. HUANG, C. K. TSE, Department of Electronic and Information Engineering, Hong Kong Polytechnic University, Hong Kong, China
(✉) e-mail: michael.tse@polyu.edu.hk
M. HUANG, School of Electronic Engineering, Wuhan University, Wuhan, China
X. RUAN, College of Automation Engineering, Nanjing University of Aeronautics and Astronautics, Nanjing, China

study, the VSCs are controlled under a typical feedback configuration that contains an outer voltage loop which operates in conjunction with a sinusoidal pulse-width-modulated (SPWM) inner current loop for achieving a constant output dc voltage, as presented in Fig. 3. The two converters have been designed separately according to their respective application conditions. However, when they are connected to the non-ideal grid, their interaction may have an impact on stability.

The stability issue of grid-connected VSCs in the presence of varying grid impedance has been discussed in several prior publications. For instance, Belkhayat [6] presented an impedance-based approach to evaluate the stability of ac interfaces in the *dq*-frame by employing a generalized Nyquist stability criterion (GNC) based on small-signal modeling. The stability of grid-connected inverters and rectifiers has also been discussed [7–9]. Moreover, a converter's impedance modeling has been studied in some detail [10–12]. Some preliminary studies of the effect of grid impedance on grid-connected interacting converters have been reported in [13–15]. Furthermore, some bifurcation phenomena have been observed and reported in some earlier studies [16–18].

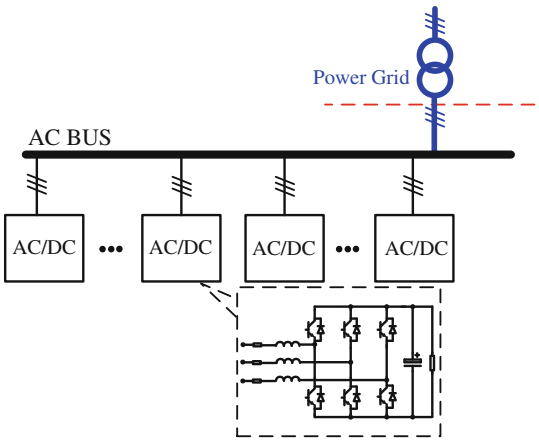

Fig. 1 Multiple voltage-source converters (VSCs) connected to power grid

In this paper, the important issue of the effect of interaction between the grid-connected converters under non-ideal power grid conditions is addressed, which is largely unexplored despite its practical importance. The study will probe into the key control parameters and examine how variation of these parameters alters the stability regions under the effect of converters' interaction. Specifically, we focus on the loss of stability corresponding to emergence of a low-frequency oscillation as commonly studied under the broad class of Hopf-type bifurcation phenomena [19]. We show that the bifurcation boundaries (stability regions from an engineering viewpoint) generally shrink when converters interact via the non-ideal grid. In other words, analysis assuming independent (uncoupled) converters under ideal grid condition therefore provides over-optimistic stability prediction. In Sect. 2, we take a quick tour of the instability phenomenon arising from converters' interaction. In Sect. 3, a detailed stability assessment employing an impedance-based approach is presented. Finally, in Sect. 4,

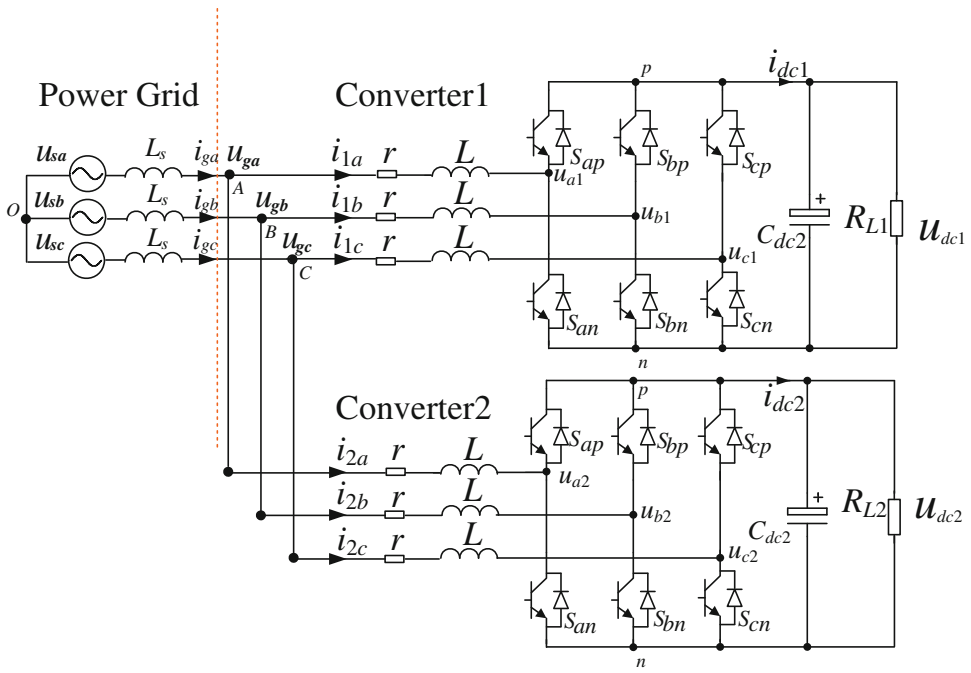

Fig. 2 Basic model of two voltage-source converters connected to the grid at the common set of points A, B and C

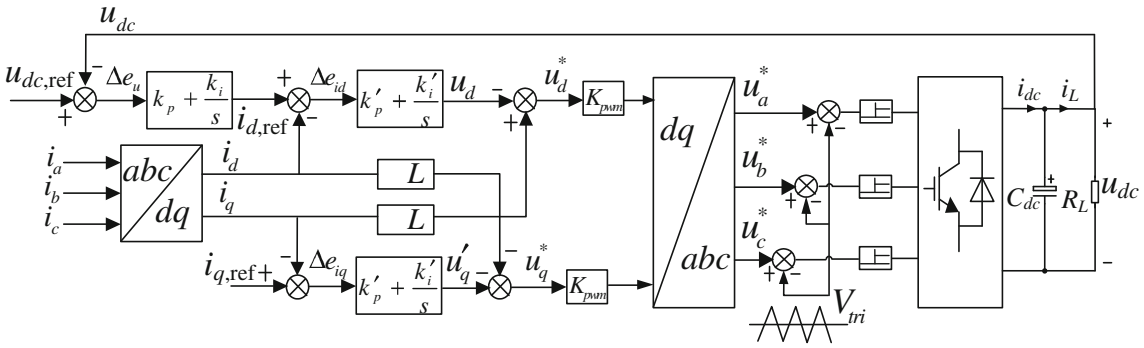

Fig. 3 Controller schematic of the three-phase voltage-source converter with filter in a rotating *dq* reference frame

we present our results in a design-oriented format that reveals the way in which stability would be affected by variation of selected parameters, and hence facilitates the choice of parameters for stable operation [20].

2 A glimpse at the instability

We begin by taking a quick glimpse at the way in which a voltage-source converter loses stability. The circuit of Fig. 2 is studied in full circuit implementation using MATLAB. The values of the circuit components used in the simulation are summarized in Tables 1, 2 and 3. Converters 1 and 2 employ the same control method which is described in Fig. 3.

Figure 4a shows stable operation of the two converters with different load conditions when separately connected to the same non-ideal grids with impedance $L_g = 1.2$ mH. Thus, the converters are stable when analyzed separately. However, when the converters are connected at the same time to the non-ideal grid having the same impedance at the *point of common coupling* (PCC), as shown in Fig. 2, the converters' output voltages and input currents have manifested low-frequency osci.

Figure 4b The dc voltage U_{dc} of both converters oscillate at 255 Hz around the regulated level, while all converters' parameters have remained the same as in the case of separate uncoupled operation.

Thus, it can be inferred that the converters could interact with each other and lose stability via a Hopf-type bifurcation when the values of parameters are selected beyond a specific region in the parameter space (referred to as stability region here).

3 Analysis

For an individual grid-connected VSC, control models and their closed-loop stability analysis have been studied [7], employing techniques like root locus analysis and Bode

Table 1 Parameters of power grid

$U_{sa,sb,sc}$	f_l	L_s
110 V rms	50 Hz	0.1–1.5 mH

Table 2 Circuit parameters of converter 1

$U_{\mathrm{dc,ref}}$	C_{dc}	L_1	R_{L1}	r	f_s
360 V	1.2 mF	3 mH	20–60 Ω	0.01 Ω	10 kHz

Note Parameters are as shown in Fig. 2 and Fig. 3

Table 3 Circuit parameters of converter 2

$U_{\mathrm{dc,ref}}$	C_{dc}	L_2	R_{L2}	r	f_s
360 V	1.2 mF	3 mH	20–60 Ω	0.01 Ω	10 kHz

Note Parameters are as shown in Fig. 2 and Fig. 3

diagrams. Moreover, the state-space approach is also used to determine stability in the time domain [15]. For grid-connected converters, prior studies [6, 21] have pointed out that the impedance-based approach is more advantageous and flexible. For the case of the grid-connected system under study, the impedance-based analysis is highly suitable, as will be demonstrated in the subsequent subsections.

3.1 Basic system model: the uncoupled case

Following the formulation of Sun [22], the three-phase VSC can be represented by an averaged model in the *dq* rotating coordinate. Since converters 1 and 2 share the same model, we provide, for brevity, the equations for converter 1 as follows:

$$\begin{cases} L_1 \frac{di_{1d}}{dt} = \omega_l L_1 i_{1q} + u_{gd} - r_1 i_{1d} - u_{1d} \\ L_1 \frac{di_{1q}}{dt} = -\omega_l L_1 i_{1d} + u_{gq} - r_1 i_{1q} - u_{1q} \\ C_{dc1} \frac{du_{dc1}}{dt} = \frac{3}{2}(d_{1d} i_{1d} + d_{1q} i_{1q}) - i_{o1} \end{cases} \quad (1)$$

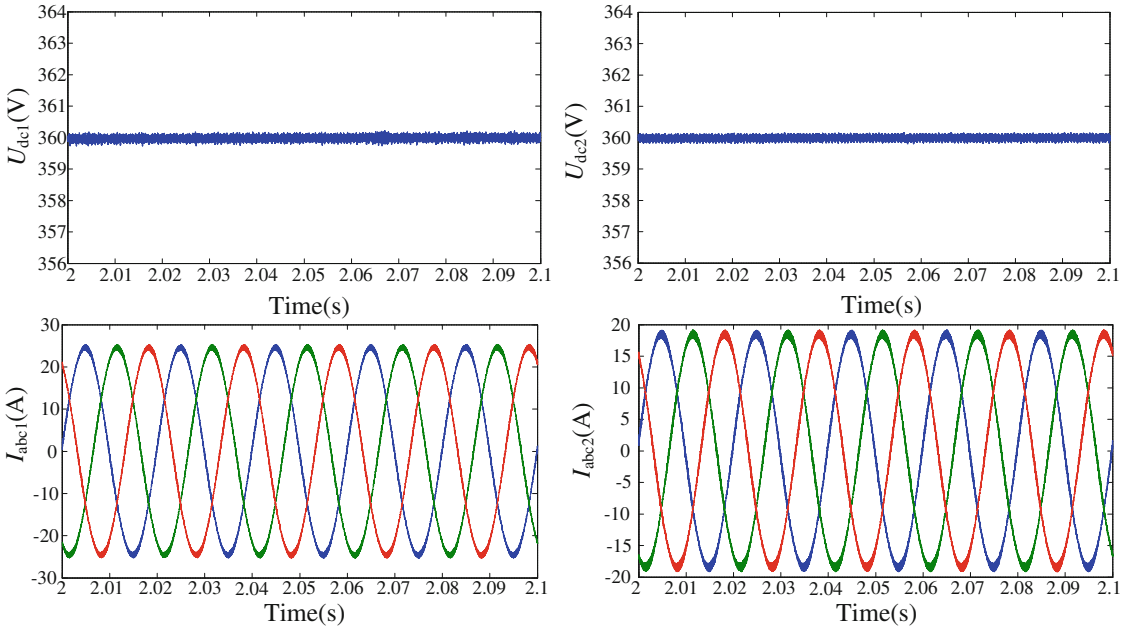

(a) The two converters work independently (with no interaction) under same grid impedance L_g =1.2 mH, showing stable operation

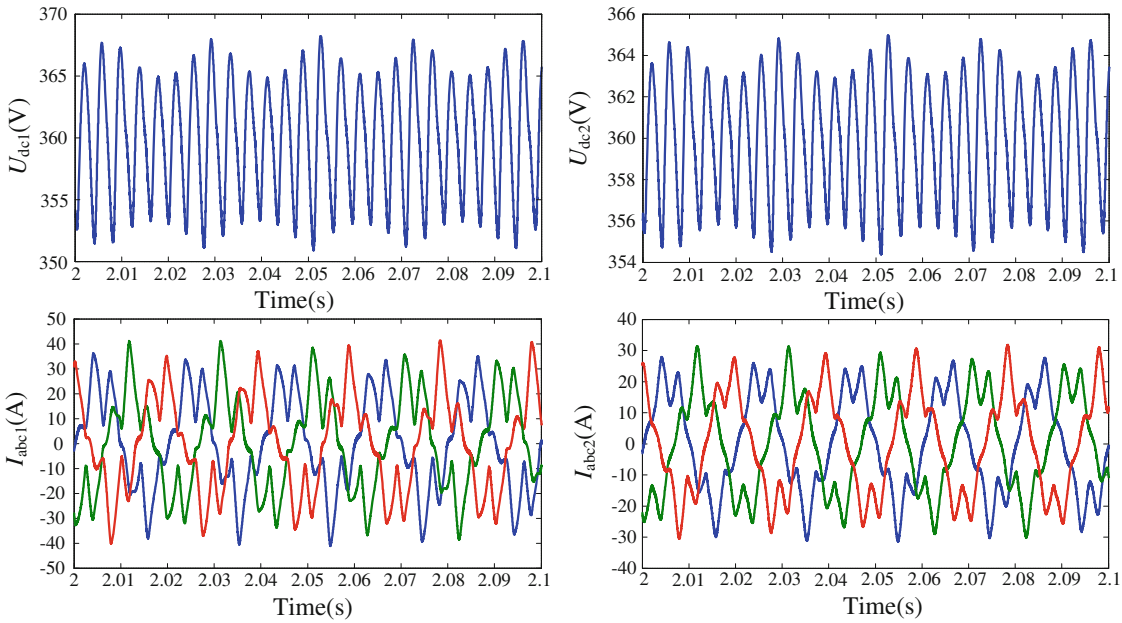

(b) The two converters interact via connecting to the non-ideal grid with L_g =1.2 mH, showing unstable operation or Hopf-type instability

Fig. 4 Waveforms of the two converters' output voltages and input currents with $R_{L1} = 22.5\ \Omega$ and $R_{L2} = 27\ \Omega$

where subscript 1 denotes converter 1 (likewise, subscript 2 denotes converter 2 in the subsequent analysis); $\omega_l = 2\pi f_l$; $d_{1d} = u_{1d}/u_{dc1}$ and $d_{1q} = u_{1q}/u_{dc1}$ are the duty cycles; i_{1d} and i_{1q} are the input currents of converter 1 in the dq-frame; u_{gd} and u_{gq} are the voltages at the point of common coupling (PCC); u_{1d} and u_{1q} are the leg voltages in the dq-frame; and i_{o1} is the load current. For simplicity, we ignore the inductor resistance r in the following analysis. From (1), we can obtain the small-signal representation via the usual linearization procedure, i.e.,

$$\begin{cases} L_1 \frac{d\hat{i}_{1d}}{dt} = \omega_l L_1 \hat{i}_{1q} - \hat{u}_{dc1} D_{1d} + \hat{d}_{1d} U_{dc1} + \hat{u}_{gd} \\ L_1 \frac{d\hat{i}_{1q}}{dt} = -\omega_l L_1 \hat{i}_{1d} - \hat{u}_{dc1} D_{1q} + \hat{d}_{1q} U_{dc1} + \hat{u}_{gq} \\ C_{dc1} \frac{d\hat{u}_{dc1}}{dt} = \frac{3}{2}\left(D_{1d}\hat{i}_{1d} + D_{1q}\hat{i}_{1q} + \hat{d}_{1d} i_{1d} + \hat{d}_{1q} i_{1q}\right) - \hat{i}_{o1} \end{cases} \tag{2}$$

where D_{1d}, D_{1q}, I_{1d}, I_{1q} and U_{dc1} are the system's steady-state values which are given by

$$\begin{cases} D_{1d} = \frac{U_{sd}}{U_{dc1}}, \\ D_{1q} = \frac{-\omega_l L_1 I_{1d}}{U_{dc1}}, \\ I_{1q} = I_{1q-ref} \text{ and} \\ U_{dc1} = U_{dc1-ref} \end{cases} \tag{3}$$

Omitting the standard small-signal derivation, the state-space representation of the closed-loop system can be obtained as

$$s\begin{pmatrix} I_{1d}(s) \\ I_{1q}(s) \\ U_{dc1}(s) \end{pmatrix} = A\begin{pmatrix} I_{1d}(s) \\ I_{1q}(s) \\ U_{dc1}(s) \end{pmatrix} + B\begin{pmatrix} U_{gd}(s) \\ U_{gq}(s) \\ I_{o1}(s) \end{pmatrix} \tag{4}$$

where

$$A = \begin{pmatrix} -\frac{G_{i1}}{L_1} & 0 & -\frac{D_{1d}}{L_1} - \frac{G_{v1}G_{i1}}{U_{dc1}} \\ 0 & -\frac{G_{i1}}{L_1} & -\frac{D_{1q}}{L_1} \\ \frac{3D_{1d}}{2C_{dc1}} + \frac{3G_{i1}I_{1d}}{2C_{dc1}U_{dc1}} & \frac{3D_{1q}}{2C_{dc1}} + \frac{3I_{1d}\omega_l L_1}{2C_{dc1}U_{dc1}} & \frac{3I_{d1}G_{v1}G_{i1}}{2C_{dc1}U_{dc1}} \end{pmatrix} \tag{5}$$

and

$$B = \begin{pmatrix} \frac{1}{L_1} & 0 & 0 \\ 0 & \frac{1}{L_1} & 0 \\ 0 & 0 & -\frac{1}{C_{dc1}} \end{pmatrix} \tag{6}$$

For brevity of presentation, we define

$$I_1 = \begin{pmatrix} I_{1d}(s) \\ I_{1q}(s) \end{pmatrix}, \quad U_g = \begin{pmatrix} U_{gd}(s) \\ U_{gq}(s) \end{pmatrix}, \quad Y_{1i} = \begin{pmatrix} \frac{1}{L_1} & 0 \\ 0 & \frac{1}{L_1} \end{pmatrix}$$

$$G_{1id} = \begin{pmatrix} -\frac{G_{i1}}{L_1} & 0 \\ 0 & -\frac{G_{i1}}{L_1} \end{pmatrix}, \quad A_{1i} = \begin{pmatrix} -\frac{D_{1d}}{L_1} - \frac{G_{v1}G_{i1}}{U_{dc1}} \\ -\frac{D_{1q}}{L_1} \end{pmatrix},$$

$$G_{1id} = \begin{pmatrix} -\frac{G_{i1}}{L_1} & 0 \\ 0 & -\frac{G_{i1}}{L_1} \end{pmatrix}, \quad A_{1i} = \begin{pmatrix} -\frac{D_{1d}}{L_1} - \frac{G_{v1}G_{i1}}{U_{dc1}} \\ -\frac{D_{1q}}{L_1} \end{pmatrix},$$

$$A_{1v} = \begin{bmatrix} \frac{3D_{1d}}{2C_{dc1}} + \frac{3G_{i1}I_{1d}}{2C_{dc1}U_{dc1}} & \frac{3D_{1q}}{2C_{dc1}} + \frac{3I_{1d}\omega_l L_1}{2C_{dc1}U_{dc1}} \end{bmatrix}$$

$$T(s) = \begin{pmatrix} G_{1id} & A_{1i} \\ A_{1v} & Z_1 \end{pmatrix}, \quad Z_{1o} = -\frac{1}{C_{dc1}},$$

$$Z_1 = \frac{3I_{d1}G_{v1}G_{i1}}{2C_{dc1}U_{dc1}}$$

The impedance function of the closed loop system can be written as

$$\begin{pmatrix} I_1 \\ U_{dc1} \end{pmatrix} = (sI - T(s))^{-1}\begin{pmatrix} Y_{1i} & O \\ O & Z_{1o} \end{pmatrix}\begin{pmatrix} U_g \\ I_{o1} \end{pmatrix} \tag{7}$$

Therefore, the characteristic polynomial that determines the stability of the closed loop system can be found as

$$\Phi_{CL}(s) = \det(sI - T(s)) \tag{8}$$

Thus, we can assess the stability of the system by inspecting the roots of $\Phi_{CL}(s) = 0$, i.e., eigenvalues of $T(s)$. Stability requires that all eigenvalues have negative real parts. Putting the parameter values in (8), we can compute the eigenvalues as given in Table 4, which indicate stable operation of the uncoupled converters.

3.2 Analysis of the interacting converters

The foregoing subsection derives the conventional converter's closed-loop model and assesses the stability of the converters when working independently (uncoupled). In this subsection, the converters are connected to the power grid at a common coupling point and thus interact with each other. As the two converters have identical control loops, from (7), we can derive the converters' impedance as

$$\begin{cases} \begin{pmatrix} I_k \\ U_{dck} \end{pmatrix} = \begin{pmatrix} Y_{ki}^{CL} & A_{ki}^{CL} \\ A_{kv}^{CL} & Z_{ko}^{CL} \end{pmatrix}\begin{pmatrix} U_g \\ I_{ok} \end{pmatrix}, \quad (k = 1, 2) \\ \begin{pmatrix} Y_{ki}^{CL} & A_{ki}^{CL} \\ A_{kv}^{CL} & Z_{ko}^{CL} \end{pmatrix} = (sI - T(s))^{-1}\begin{pmatrix} Y_{ki} & O \\ O & Z_{ko} \end{pmatrix} \end{cases} \tag{9}$$

Combining (9) and $I_o = U_{dc}/R_L$, we obtain the input admittance of each converter as seen at the coupling point, i.e.,

Table 4 Eigenvalues of the uncoupled converters (independently operated)

Systems	Eigenvalues	Stability
Converter 1	−1528.885 ± j2889.817, −4.168, −4.199, −7995.83, −8.029	Stable
Converter 2	−1936.886 ± j2622.119, −4.168, −4.199, −7995.83, −8.067	Stable

$$\begin{cases} Y_{VSCk} = Y_{ki}^{CL} + \frac{A_{ki}^{CL} A_{kv}^{CL}}{R_{Lk} - Z_{ko}^{CL}}, \quad (k = 1, 2) \\ Y(s) = Y_{VSC1} + Y_{VSC2} \end{cases} \tag{10}$$

where Y_{VSCk} ($k = 1, 2$) is the converter's input admittance and $Y(s)$ is the total input admittance of the two converters.

In a likewise manner, the grid impedance can be found from

$$Z_s I_s = U_s - U_g \tag{11}$$

where

$$\begin{cases} I_s = \begin{pmatrix} I_{sd} \\ I_{sq} \end{pmatrix}, \\ U_s = \begin{pmatrix} U_{sd} \\ U_{sq} \end{pmatrix}, \\ Z_s = \begin{pmatrix} L_s s & -\omega_l L_s \\ \omega_l L_s & L_s s \end{pmatrix} \end{cases} \tag{12}$$

Thus, the system's impedance can be considered in the usual Thevenin form, as shown in Fig. 5.

Based on this small-signal model, the current I_s from power grid to the coupled converters is

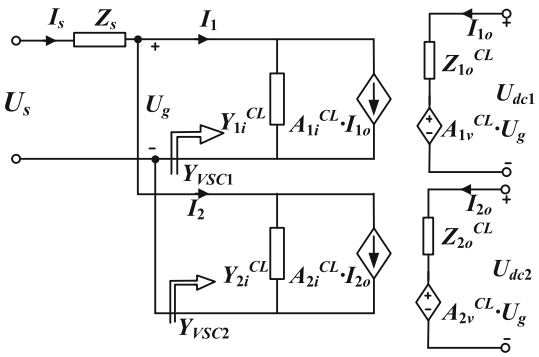

Fig. 5 Impedance model of the system of interacting converters in *dq*-frame

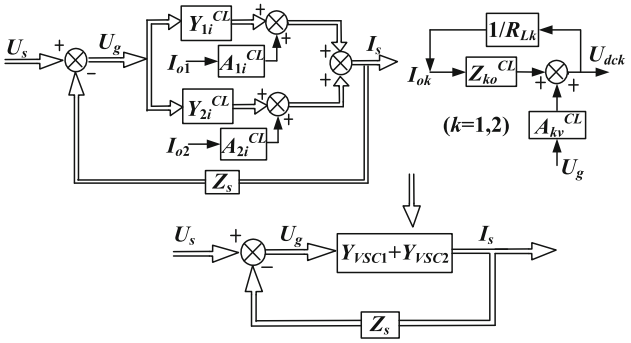

Fig. 6 Block diagram of the impedance model of the system of interacting converters in *dq*-frame

$$I_s = \frac{Y(s)}{I + Y(s)Z_s} U_s \tag{13}$$

Since the converters are stable when operating independently, both U_s and $Y(s)$ are stable and the stability of the connected system can be assessed by applying Nyquist criterion [23] to (Fig. 6)

$$H(s) = \frac{1}{I + Y(s)Z_s} \tag{14}$$

The Nyquist plot of $\det(I + Y(s)Z_s)$, as given in Fig. 7, shows encirclement of the origin which asserts that the system is unstable. Numerical calculations of the poles of the closed-loop system also indicate unstable operation, as shown in Table 5. This result is in full agreement with the simulations presented earlier.

For a general system with multi-converters connected to a non-ideal power grid at the same PCC as shown in Fig. 1, we can track the trajectory to determine the overall system's stability. The total input admittance of the connected system is $Y_{VSC} = Y_{VSC1} + Y_{VSC2} + Y_{VSC3} + \ldots + Y_{VSCn}$, and the impedance in *dq*-frame could be obtained as shown in Fig. 8. The stability could be assessed by examining the root locus of $\det(I + Y_{VSC}Z_s)$.

The above analysis clearly exposes that the interacting converters can be unstable while the individual separately operated converters are stable.

4 Stability regions in design-oriented forms

In the foregoing analysis, the system's stability has been determined precisely using the interface impedance. However, for engineering design purposes, it is more important to identify the system parameters and their variation trends that have significant impact on the stable region of operation [20, 24]. In this section, we derive stability boundaries using the foregoing analysis and present them in design-oriented forms. Results from simulations of the actual switching circuits will also be presented for comparison and verification.

Relevant to our present study is the region of stable operation bounded by the bifurcation boundary corresponding to the loss of stability via a Hopf-type bifurcation (practically known as low-frequency oscillation). For the system of two converters connected to a non-ideal power grid, we focus on the following parameters:

1) the grid impedance L_g,
2) the dc gains of the two converters' voltage loop k_{vp1}, k_{vp2},
3) the converters' load resistance R_{L1}, R_{L2}.

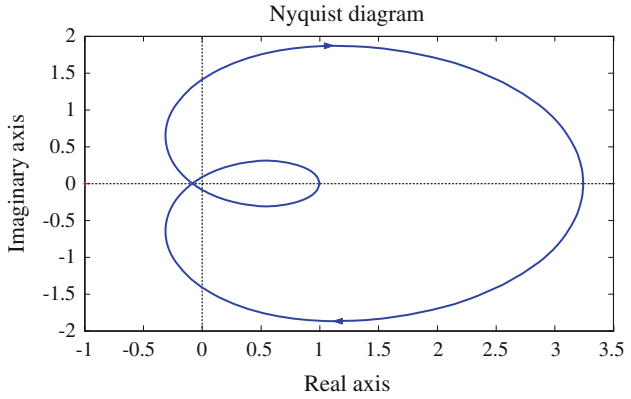

Fig. 7 Nyquist diagram of the system of interacting converters

Table 5 Eigenvalues of the system of interacting converters

Systems	Eigenvalues	Stability
Connected systems	61.616 ± j2439.676, −1749.02 ± j2739.079, −4433.38, −4.19 ± j0.011, −4.168, −4.199, −7995.83, −8.03, −8.06	Unstable

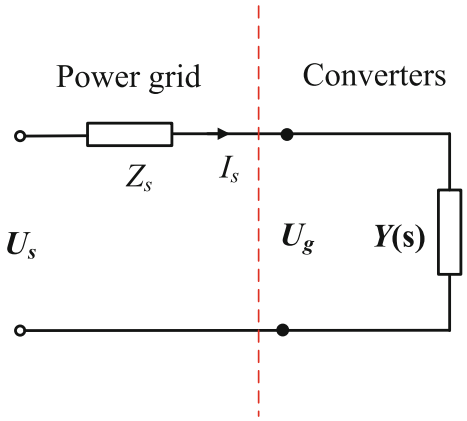

Fig. 8 Thevenin equivalent circuit of multiple VSCs connected to a non-ideal power grid at the same coupling point

Moreover, for the purpose of comparison, the stability regions of converters coupled via the power grid and those of the independently operating (uncoupled) converters are presented. Our results are generated from simulations of the complete switching model which provides viable verification of the actual physical system.

In the sequel, we will present a series of design-oriented stability charts which are computed from the analysis of Sect. 3 and also from full circuit simulations. Each chart contains two sets of stability boundaries, shown in red and blue, corresponding to two specific parameter values as labelled in the chart. In each chart, for the red or blue set of boundaries, the parameter plane is divided into regions I, II and III.

Region I (stable) is the parameter region where the system is stable for both cases of independently operated converters and grid-coupled converters.
Region II (intermediate) is the parameter region where the independently operated converters are stable, but the system of grid-coupled converters is unstable.
Region III (unstable) is the parameter region where the system is unstable for both cases of independently operated converters and grid-coupled converters

Thus, the boundary separating regions I and II is the bifurcation boundary or stability threshold for the system of coupled converters, and the boundary separating regions II and III is the bifurcation boundary for the independently operated converter. In each chart, analytically calculated stability boundaries are plotted in asterisk (*), and the corresponding full circuit simulated boundaries are shown in solid curves.

The dc gains of voltage loop k_{vp1}, k_{vp2} are the key parameters that affect stability with respect to Hopf bifurcation. Since the inner current loop gain is usually chosen to be sufficiently high to ensure that the current tracks the reference closely, we will ignore the inner loop gain in our study. For the system of converters connected at the same PCC, the stability regions in the k_{vp1}–k_{vp2} plane is shown in Fig. 9, for both the uncoupled and coupled systems for different values of dc loads and grid impedance. These charts reveal how variation of these parameters would affect the stability regions, and specifically we see that the stable operating regions are reduced when either dc load current, line impedance or dc link capacitor is increased.

The dc load resistance of the converters can affect stability, as shown in the design-oriented charts of Fig. 10. From the charts presented in Fig. 10, when one converter is more heavily loaded, the system moves closer to the boundary of instability. Moreover, we observe that the region of stability shrinks when the converters are coupled via the on-ideal grid.

From the charts presented above, we see that the analytically computed boundary points are in perfect agreement with the full-circuit simulated results. The effects of different parameters on the overall system stability can be summarized qualitatively in Table 6. Specifically, the system would alter the stability margin when parameters vary. In the table, the ‘‘ + ’’ and ‘‘−’’ signs indicate increasing and decreasing values of the parameters, respectively. Correspondingly, the sign ‘‘↑’’ means enlarging the overall system stability margin, whereas ‘‘↓’’ represents reducing the stability margin. For instance, when the load decreases (−), the overall system stability region shrinks (↓), and vice versa.

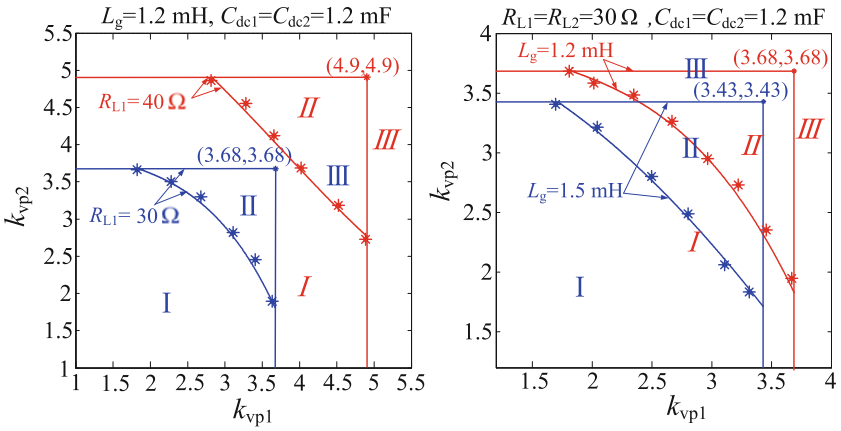

(a) Variation of converter 1's dc load R_{L1} with R_{L2}=R_{L1}

(b) Variation of grid impedance L_g with R_{L1}=R_{L2}=30 Ω

Fig. 9 Stability boundaries on the 2-dim plane of dc gains, i.e., k_{vp1} versus k_{vp2}. Points (*) are calculated from analysis of Sect. 3, and *solid curves* are from full circuit simulations

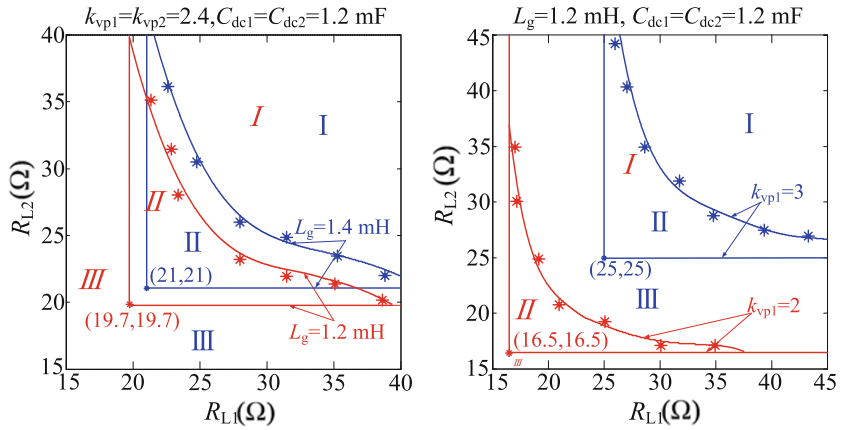

(a) Variation of grid impedance L_g with k_{vp1}=k_{vp2}=2.4

(b) Variation of dc gain of converter's voltage loop with k_{vp1}=k_{vp2}.

Fig. 10 Stability boundaries on the 2-dim plane of load resistances, i.e., R_{L1} versus R_{L2}. Points (*) are calculated from analysis of Sect. 3, and solid curves are from full circuit simulations

Table 6 Effects of system's parameters on stability regions

Parameters	Variation	Stability margin
Dc gain of voltage loop	− +	↑ ↓
Converter's load	− +	↓ ↑
Grid impedance	− +	↑ ↓

Note The '' + '' and ''−'' signs indicate increasing and decreasing values of the parameters, respectively. Correspondingly, ''↑'' means enlarging the overall system stability margin and ''↓'' represents reducing the stability margin

5 Conclusion

Power converters connected to a non-ideal power grid are studied in this paper. The emphasis is on the mutual interaction of two or more converters via the grid and how such interaction may cause instability of the overall system. The study is important as converters are being increasingly deployed for applications involving power conversion functions that require interfacing with power grid which is often non-ideal. The significant impedance present in the grid poses an issue deserving attention as converters' stability is no longer a standalone problem. Through mutual interaction, converters become more prone to instability under certain conditions. This paper points out that the overall system stability should be re-considered in the light of a more complete model that takes into account the interaction of converters connected to the grid at a common point of coupling. The analysis has been developed using the impedance approach, and stability boundaries are derived in various parameter planes. Findings

reported in this paper would facilitate engineers in making design choices related to the selection of parameter values that would guarantee stability in a sufficiently wide parameter range.

Acknowledgment The work was supported by Hong Kong Polytechnic University Grants G-U866 and G-YJ32.

References

[1] Sanjuan S (2010) Voltage oriented control of three-phase boost PWM converters. Master Thesis, Chalmers University of Technology, Gothenburg, Sweden
[2] Wang XF, Guerrero JM, Chen Z et al (2010) Distributed energy resources in grid interactive AC microgrids. In: Proceedings of the 2nd IEEE international symposium on power electronics for distributed generation systems (PEDG'10), 16–18 June 2010, Heifei, China, pp 806–812
[3] Areerak KN, Bozhko SV, Asher GM et al (2012) Stability study for a hybrid ac–dc more-electric aircraft power system. IEEE Trans Aerosp Electr Syst 48(1):329–347
[4] Ciezki JG, Ashton RW (2000) Selection and stability issues associated with a navy shipboard dc zonal electric distribution system. IEEE Trans Power Deliv 15(2):665–669
[5] Ariyasinghe DP, Vilathgamuwa DM (2008) Stability analysis of microgrids with constant power loads. In: Proceedings of the IEEE international conference on sustainable energy technology (ICSET'08), 24–27 Nov 2008, Singapore, pp 279–284
[6] Belkhayat M (1997) Stability criteria for ac power systems with regulated loads. Ph.D. Dissertation, Purdue University, West Lafayette, IN, USA
[7] Sun J (2011) Impedance-based stability criterion for grid-connected inverters. IEEE Trans Power Electron 26(11):3075–3078
[8] Burgos R, Boroyevich D, Wang F et al (2010) On the ac stability of high power factor three-phase rectifiers. In: Proceedings of the IEEE energy conversion congress and exposition (ECCE'10), 12–16 Sept 2010, Atlanta, GA, USA, pp 3075–3078
[9] Belkhayat M, Cooley R, Abed EH (1995) Stability and dynamics of power systems with regulated converters. In: Proceedings of the IEEE international symposium on circuits and systems (ISCAS'95), vol 1, 30 Apr–3 May 1995, Seattle, WA, USA, pp 143–145
[10] Harnefors L, Bongiorno M, Lundberg S (2007) Input-admittance calculation and shaping for controlled voltage-source converters. IEEE Trans Power Electron 54(6):3323–3334
[11] Cespedes M, Sun J (2012) Impedance shaping of three-phase grid-parallel voltage-source converters. In: Proceedings of the 27th annual IEEE applied power electronics conference and exposition (APEC'12), 5–9 Feb 2012, Orlando, FL, USA, pp 754–760
[12] Huang J, Corzine K, Belkhayat M (2007) Single-phase ac impedance modeling for stability of integrated power systems. In: Proceedings of the 2007 IEEE electric ship technologies symposium (ESTS'07), 21–23 May 2007, Arlington, VA, USA, pp 483–489
[13] Chandrasekaran S, Boroyevich D, Lindner DK (1999) Input filter interactions in three phase ac–dc converters. In: Proceedings of the 30th annual IEEE power electronics specialists conference (PESC'99), vol 2, 26 June–2 July 1999, Charleston, SC, USA, pp 987–992
[14] Wan C, Huang M, Tse CK et al (2013) Nonlinear behavior and instability in a three-phase boost rectifier connected to a non-ideal power grid with an interacting load. IEEE Trans Power Electron 28(7):3255–3265
[15] Huang M, Tse CK, Wong SC et al (2013) Low-frequency Hopf bifurcation and its effects on stability margin in three-phase PFC power supplies connected to non-ideal power grid. IEEE Trans Circ Syst I Regul Papers. doi:10.1109/TCSI.2013.2264698
[16] Suto Z, Nagy I (2003) Analysis of nonlinear phenomena and design aspects of three-phase space-vector-modulated converters. IEEE Trans Circ Syst I: Fundam Theory Appl 50(8):1064–1071
[17] Dai D, Li S, Ma X et al (2007) Slow-scale instability of single-stage power-factor-correction power supplies. IEEE Trans Circ Syst I Regul Papers 54(8):1724–1735
[18] Xiong X, Tse CK, Ruan X (2013) Bifurcation analysis of standalone photovoltaic-battery hybrid power system. IEEE Trans Circ Syst I Regul Papers 60(5):1354–1365
[19] Tse CK (2003) Complex behavior of switching power converters. CRC Press, Boca Raton, FL, USA
[20] Tse CK, Li M (2011) Design-oriented bifurcation analysis of power electronics systems. Int J Bifurc Chaos 21(6):1523–1539
[21] Harnefors L, Bongiorno M, Lundberg S (2007) Input-admittance calculation and shaping for controlled voltage-source converters. IEEE Trans Ind Electron 54(6):3323–3334
[22] Sun J (2009) Small-signal methods for ac distributed power systems—a review. IEEE Trans Power Electron 24(11):2545–2554
[23] Macfarlane AGJ, Postlethwaite I (1977) The generalized Nyquist stability criterion and multivariable root loci. Int J Control 25(1):81–127
[24] Rodriguez E, El Aroudi A, Guinjoan F et al (2012) A ripple-based design-oriented approach for predicting fast-scale instability in DC-DC switching power supplies. IEEE Trans Circ Syst I Regul Papers 59(1):215–227

Author Biographies

Cheng WAN received the B.Eng. in Hydropower engineering from Wuhan University in 2009. Currently he is pursuing a Ph.D. degree in power electronics at Huazhong University of Science and Technology. His research interests include bifurcation of converters, nonlinear control and applications.

Meng HUANG received the B.Eng. and M.Eng degree in electronics science and technology from the Huazhong University of Science and Technology, Wuhan, China, in 2006 and 2008, respectively, and the Ph.D. degree from the Department of Electrical and Information Engineering, Hong Kong Polytechnic University.

Chi K. TSE received the B.Eng. (first class Hons) degree in electrical engineering and Ph.D. degree from the University of Melbourne, Melbourne, Australia, in 1987 and 1991, respectively. He is currently a Chair Professor of the Department of Electronic and Information Engineering, Hong Kong Polytechnic University, Hong Kong.

Xinbo RUAN received the B.S. and Ph.D. degree in electrical engineering from Nanjing University of Aeronautics and Astronautics (NUAA), Nanjing, China, in 1991 and 1996, respectively. He is currently the vice-dean of the College of Automation Engineering, Nanjing University of Aeronautics and Astronautics, Nanjing.